Results Obtained with a New Instrument for the Measurement of Particle Size Distributions from Diffraction Patterns

Michael Heuer, Kurt Leschonski *

(Received: 12 October 1984)

Abstract

For several years the size distributions of particulate matter have increasingly been determined by using diffraction pattern analysis.
In order to evaluate particle size distributions from the far field intensity distribution of light diffracted by a distribution of particles, a linear set of equations must be solved. Since, in many cases of application, conventional methods for solving linear sets of equations become unstable, the calculated particle size distribution may also be grossly in error. By applying special, known mathematical methods we succeeded in obtaining a parameter-free solution of the above problem.
After a brief description of the mathematical method used, a diffraction pattern analyser will be presented as well as some experimental results obtained with it. The results obtained with aerosols and suspensions come from experiments performed with narrow-sized latexes and mono- and bi-modal particle size distributions of limestone and quartz.

1 Introduction

For a number of years optical methods have increasingly been used for the measurement of particle size distributions. The variable used to measure the size of an individual particle, an average size, or the size distribution is the light scattered into a certain angle of space. Modern electronic and computer technology have made it possible to analyse particle size distributions quicker and more reproducibly than with other known methods. On the other hand, the existing gap between the theory of these instruments, which is based on spherical particles, and the measurement of particles of irregular shape cannot yet be closed. Comparative tests with other methods of particle size analysis do not, therefore, always yield the results one would expect. This, however, does not reduce the interest which these instruments now receive, due to the fact that speed, reproducibility, and simple handling are in many cases much more interesting than absolute accuracy. The report covers the development of a new diffraction pattern analyser. The analyser has been built for non-interruptive, online particle size measurements in two-phase flow systems. An instrument of this type was needed for the investigation of the movement of fine particles in gas and liquid flows as encountered in classifiers, separators and dryers. Since commercially available equipment could not be adapted to our problems, a high resolution diffraction pattern analyser was developed.

2 Principle and Basic Equation

The physical principle of a diffraction pattern analyser, used for particle size analysis, has been well known for many years. In 1817 *Fraunhofer* [1] described a system for producing diffraction patterns similar, with the exception of the light source used, to the one shown in Figure 1.

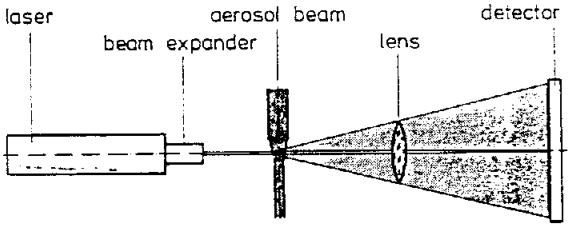

Fig. 1: Optical setup for the measurement of diffraction patterns.

If one illuminates monosized circular, or spherical, particles in an extended laser beam, a radially symmetric diffraction pattern will be obtained in the focal plane of the lens. The particles may be stationary or moving, suspended in a gas or a liquid; the diffraction pattern remains the same. It consists of an extremely bright centre and a series of concentric dark and bright rings. The intensity distribution, $I(r, x)$, as obtained on the detector surface, was first described by *Airy* [2] in 1835 with a formula similar to Eq. (1). This equation represents the Fraunhofer approximation for $\theta < 8°$ with $tg\,\theta = r/f$.

$$I(r, x) = I_0(k x^2/2)^2 \, (J_1(krx)/(krx))^2 \tag{1}$$

with

$$k = (\pi/\lambda f) \, . \tag{2}$$

f represents the focal length of the lens, λ the wavelength of the monochromatic light used. I_0 is the intensity of the incident light beam and J_1 the first order Bessel-function of the first kind. The diffraction theory shows that the bigger the radius, r_0, of the

* Dipl.-Ing. *M. Heuer*, Prof. Dr.-Ing. *K. Leschonski*, Institut für Mechanische Verfahrenstechnik der Technischen Universität Clausthal, Leibnizstraße 15, D-3392 Clausthal-Zellerfeld (Federal Republic of Germany).

0176-2265/85/0105-0007 $02.50/0

smallest, that is the first, dark ring the smaller the diameter, x, of the circular or spherical particles. r_0 can be calculated from:

$$r_0 = 1.22 \frac{\lambda f}{x} . \tag{3}$$

If the spheres present in the laser beam follow a number density distribution, $q_0(x)$, the diffraction patterns of individual particles are superimposed and one obtains a radially symmetrical but diffuse diffraction pattern, $I(r)$. Assuming a continuous function for $q_0(x)$, the radial intensity distribution of the diffraction pattern can be described by:

$$I(r) = \int_{x_{min}}^{x_{max}} N_{tot}\, q_0(x)\, I(r, x)\, dx . \tag{4}$$

Eq. (4) represents a first order Fredholm integral equation of the first kind, similar to the equations one obtains when analysing the spectral extinction of a particle size distribution or the angle dependent intensity of the scattered light.
The solution of this integral equation is the number density distribution, $q_0(x)$, of the particles. As far as known, Eq. (4) was first solved in 1955 by *Chin* et al. [3, 4] and in 1956 by *Shifrin* [5] by the application of the so-called Mellin transformation first suggested in 1924 by *Titchmarsh* [6]. Similar but different solutions have been suggested by *Shifrin* and *Kolmakov* [7]. An approximate solution can be obtained by the so-called numerical quadratur as described by *Twomey* [8] in 1963.
The Fredholm integral equation is transferred into a system of linear equations which can be solved as described in the following section.

3 Numerical Quadratur of the Integral Equation

The radially symmetrical diffraction pattern must be measured with a special detector. One may use, for instance, a multielement detector as shown schematically in Figure 2. It consists of concentric half circles of increasing radial width, Δr_j.

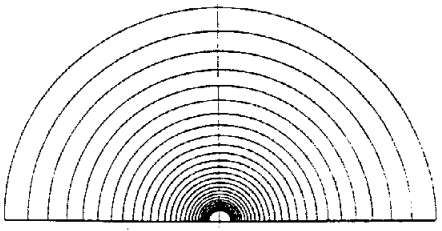

Fig. 2: Multi element detector for the measurement of radially symmetrical diffraction patterns.

The power of the light, $L(\Delta r_j)$, to be measured in the circular detector rings of width $\Delta r_j = r_{j+1} - r_j$, can be obtained by integrating the intensity distribution $I(r)$ (Eq. 4) over the area of the circular ring. One obtains:

$$L(\Delta r_j) = \int_{x_{min}}^{x_{max}} N_{tot}\, q_0(x)\, L(\Delta r_j, x)\, dx . \tag{5}$$

With

$$L(\Delta r_j, x) = (\pi/2)\, I_0 x^2 \left(J_0^2(kxr_j) + J_1^2(kxr_j) - J_0^2(kxr_{j+1}) - J_1^2(kxr_{j+1})\right). \tag{6}$$

Eq. (5) cannot be solved analytically for chosen number density distributions $q_0(x)$. A solution can, however, be found under the following assumptions: Firstly the integral of Eq. (5) is split into M particle size intervals.

$$L(\Delta r_j) = \sum_{i=1}^{M} \int_{x_i}^{x_{i-1}} N_{tot}\, q_0(x)\, L(\Delta r_j, x)\, dx . \tag{7}$$

The number density distribution $q_0(x)$ can be assumed to be constant in each interval if each individual size interval is sufficiently small. $q_0(x)$ is then replaced by the histogram $\bar{q}_0(\bar{x}_i)$, with $\bar{x}_i$ the arithmetic mean of the interval boundaries x_i and x_{i+1}. One arrives at:

$$L(\Delta r_j) = \sum_{i=1}^{M} N_{tot}\, \bar{q}_0(\bar{x}_i) \int_{x_i}^{x_{i+1}} L(\Delta r_j, x)\, dx . \tag{8}$$

If the diffraction pattern is measured in M different detector rings, Eq. (8) can be given for each individual ring. One obtains, therefore, a linear set of equations with the coefficients $L(\Delta r_j, x_i)$ which has to be solved with respect to the unknown values $\bar{q}_0(\bar{x}_i)$ of the number density distribution.

4 Special Approach for a Final Solution

If one tries to solve the linear set of equations with conventional mathematical methods, one soon realizes that extremely small fluctuations of $L(\Delta r_j)$ lead to results with no physical sense. This problem becomes more and more pronounced the higher the resolution one intends to obtain. The results of the calculations may become an oscillating curve which does not even remotely resemble the exact solution. The oscillations become larger the greater the number of equations and the fluctuations of $L(\Delta r_j)$. Figure 3 shows an example. The power of the light, $L(\Delta r_j)$, obtained by introducing a log-normal number distribution into Eq. (8) has been used to recalculate $\bar{q}_0(\bar{x}_i)$ from the same equation. The oscillating, meaningless curve shown in Figure 3 was obtained.

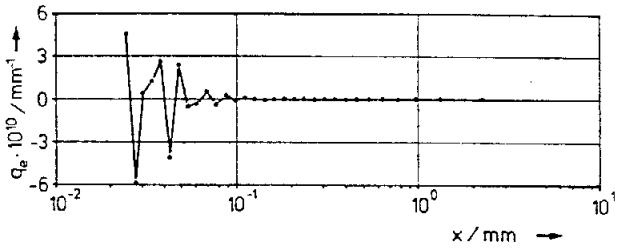

Fig. 3: Oscillating recalculated log-normal number distribution.

It can be shown, both theoretically and experimentally, that a reduction of the experimentally induced fluctuations of $L(\Delta r_j)$ is not sufficient to arrive at reasonable results. This is due to the fact that a system of linear equations, as obtained in the present case, is in principle highly unstable or ill conditioned.
If the power of the light, $L(\Delta r_j)$, is called vector L with elements L_j, the power of the light, $L(\Delta r_j, x_i)$, the coefficient matrix, A, with elements A_{ij} and the number density distribution, $\bar{q}_0(\bar{x}_i)$, Eq. (8) can be written as a matrix equation:

$$A\, q = L . \tag{9}$$

The true, but oscillating solutions q_e of Eq. (9) one obtains from:

$$q_e = A^{-1} L_f \,. \tag{10}$$

L_f represents the vector of the light power, L_j, with errors.
The oscillations described become smaller the lower the number of equations. If one restricts the number of equations to eight or ten, reasonable results can be obtained with a resolution which matches many practical applications. The matrix of coefficients, A, must then, however, be averaged over fairly wide size intervals.
If one uses a larger number of equations, the oscillations may be suppressed by two methods.
A first possibility is to postulate an analytical function as a solution for the unknown distribution curve, the parameters of which can be calculated using a least squares method. One may, for instance, use the well known distribution functions of the Gaudin-Schuhmann, the Rosin-Rammler-Sperling-Bennet or the log normal-distribution types. The field of solutions is, however, drastically reduced since a general, parameterfree solution is no longer possible. The deviations from the particle size distribution under investigation may be especially large if the analytical function chosen simulates a monomodal distribution, while in reality a bimodal or multimodal distribution exists.
We prefer, therefore, methods which, on the one hand, permit a general, parameter-free solution but on the other hand suppress oscillations. A method of this kind was suggested in 1962 by *Philipps* [9] and improved by *Twomey* [10] in 1963. *Heuer* [11] has recently published results obtained when applying *Twomey's* method to the calculation of particle size distributions from diffraction patterns.
This method accepts a certain error vector, e, with the elements e_j, when measuring the light power L. One rewrites Eq. (9), therefore, as follows:

$$A\,q_g - L_f = e \,. \tag{11}$$

In order to obtain an appropriate solution for q_g, one first forms the sum of all errors squared and arrives at:

$$(A\,q_g - L_f)^T\,(A\,q_g - L_f) = e^2 \,. \tag{12}$$

By applying the least squares method one again obtains a true, but oscillating, solution q_e. For a smoothed solution a deviation a_i is introduced, as defined in Figure 4:

$$a_i = -\frac{1}{2}\,q_{i-1} + q_i - \frac{1}{2}\,q_{i+1} \,. \tag{13}$$

a_i represents the deviation of the straight line connecting the points P_{i-1} and P_{i+1} from the ordinate of P_i. The sum of squares of these deviations equals:

$$a^2 = \sum a_i^2 = \sum \frac{1}{4}\,(2\,q_i - q_{i-1} - q_{i+1})^2 \,. \tag{14}$$

Written in a vectorial form one arrives at:

$$a = Kq \tag{15}$$

with the following matrix for K:

$$K = \begin{pmatrix} 0 & 0 & 0 & 0 & 0 \\ -1 & 2 & -1 & 0 & 0 \\ 0 & -1 & 2 & -1 & 0 \\ 0 & 0 & -1 & 2 & -1 \\ . & . & . & . & . \end{pmatrix} \tag{16}$$

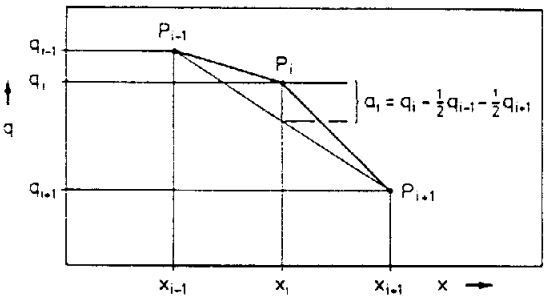

Fig. 4: Definition of the deviation a.

a^2 may be obtained from:

$$a^2 = q^T K^T K q = q^T H q \tag{17}$$

with H the product of $K^T K$

$$H = \begin{pmatrix} 1 & -2 & 1 & 0 & 0 & 0 & . \\ -2 & 5 & -4 & 1 & 0 & 0 & . \\ 1 & -4 & 6 & -4 & 1 & 0 & . \\ 0 & 1 & -4 & 6 & -4 & 1 & . \\ . & . & . & . & . & . & . \end{pmatrix} . \tag{18}$$

The sum of the squares of the errors, e, and the deviations, a, is defined as shown in Eq. (19).

$$\sum e_i^2 + \gamma \sum a_i^2 = e^2 + \gamma a^2 \,. \tag{19}$$

γ represents a weighting factor. If one introduces Eqs. (12) and (17) one obtains:

$$(A\,q_g - L_f)^T\,(A\,q_g - L_f) + \gamma\,q_g^T H q_g = e^2 + \gamma a^2 \,. \tag{20}$$

The minimization of Eq. (20) finally yields:

$$q_g = (A^T A + \gamma H)^{-1} A^T L_f \,. \tag{21}$$

This method is analogous to the method of linear optimization and the factor, γ, can therefore also be called a Lagrangian multiplier. It is a measure of the degree of smoothing. *Heuer* [11] has performed a number of mathematical simulations in order to evaluate the useful range of γ-values.
Figure 5 shows a log-normal distribution with a median value of 200 µm and a standard deviation of $s = 0.5$. Its radial intensity distribution was calculated, substituted into Eq. (2) and, with varying numerical values for γ, was then solved for $q_0(x)$. The result of this calculation is shown in Figure 6.

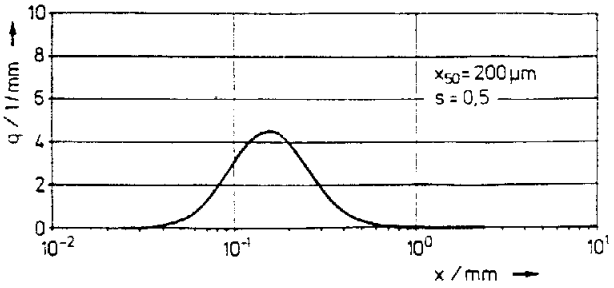

Fig. 5: Log-normal-distribution with a median particle size of 200 µm and standard deviation $s = 0.5$.

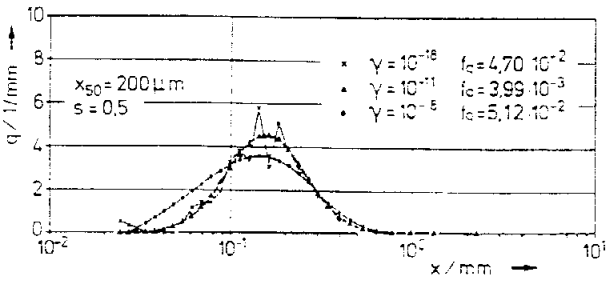

Fig. 6: Recalculated log-normal-distributions using different values of γ with sums of squared errors.

One recognizes that the best reproduction of the given log-normal distribution is obtained for $\gamma = 10^{-11}$. The sum of the squares of the errors, f_q, which was used for quantitative comparison of the back-calculated and the given distribution,

$$f_q = \sqrt{\Sigma\,(\Delta q_i \Delta x_i)^2} \tag{22}$$

amounted to $f_q = 3.99\,10^{-3}$ in this case. From these calculations it was determined that $2 \cdot 10^{-2}$ can be taken as the upper error limit. If f_q is less than 10^{-2}, the deviations lie in the region of the thickness of the lines used in Figure 6.

Heuer [11] was able to show that the curves f_q have pronounced minima in the region $10^{-13} = \gamma = 10^{-9}$ when one changes, for example, the median value of the given log-normal distribution. Those interested in further results of the simulation calculations are referred to the quoted paper [11].

The results of the simulation calculations and the experimental verification showed that one may use one single γ-value over a wide range of particles sizes. This γ-value can be experimentally determined and can then be used for subsequent analyses.

Furthermore, a decisive improvement in the necessary smoothing was obtained through an improvement in the structure of the entire matrix. It is known that a system of equations is more stable the higher the value of the determinant of the coefficient matrix. This is the case when the numerical values of the terms of the matrix around the main diagonal are largest and are not too different from each other. However, the structure of the coefficient matrix is given by $L(\Delta r_j, x_i)$. A change is only possible when one converts the number distribution to a distribution with respect to a different quantity.

The type of density distribution can be changed according to Eq. (23) [12]:

$$q_t(x) = \frac{x^{t-r} q_r(x)}{M_{t-r,r}} \,. \tag{23}$$

Here, $M_{t-r,r}$ is the complete $(t-r)-th$ moment of the $q_r(x)$-distribution and is defined according to Eq. (24):

$$M_{t-r,r} = \int_{x_{min}}^{x_{max}} x^{t-r} q_r(x)\, dx \,. \tag{24}$$

With $t = 0$ (number distribution) one obtains:

$$q_0(x) = \frac{x^{-r} q_r(x)}{M_{-r,r}} \,. \tag{25}$$

Substituting Eq. (25) into Eq. (5), one arrives at:

$$L(\Delta r_j) = N_{tot} M_{-r,r}^{-1} \int_{x_{min}}^{x_{max}} x^{-r} q_r(x)\, L(\Delta r_j, x)\, dx \,. \tag{26}$$

In the following, the constant $N_{tot}/M_{-r,r}$ will not be pursued since it disappears during the normalization of the calculations. In Eq. (26), $r = 3$ should be inserted for the calculation of a volume density distribution. For a surface area distribution, $r = 2$. For a length distribution: $r = 1$.

For $r = 3$ one obtains from Eq. (26):

$$L(\Delta r_j) = N_{tot}\, M_{-3,3}^{-1} \int_{x_{min}}^{x_{max}} x^{-3} q_3(x)\, L(\Delta r_j, x)\, dx \,. \tag{27}$$

If one, furthermore, considers $L(\Delta r_j, x)$ according to Eq. (6), one finally obtains:

$$L(\Delta r_j) = C \int_{x_{min}}^{x_{max}} q_3(x) x^{-1} \left(J_0^2(kxr_j) + J_1^2(kxr_j) - J_0^2(kxr_{j+1}) - J_1^2(kxr_{j+1})\right) dx \,. \tag{28}$$

In Figure 7 the matrices for the types of quantity $r = 0$ and $r = 3$ are represented in a three dimensional plot.

The numerical values of the coefficients correspond to the points of intersection of the lines presented. Both matrices are plotted, with dependence on radius, r, and particle size, x, on logarithmically divided axes. For both matrices one can discern a smooth surface to the right and a wave structure to the left of the main diagonals. In the region of the smooth surface the detector radii lie within the major maximum, that is the zero order of the diffraction picture of the particle. The wave structure to the left of the main diagonal is produced through the minima and maxima

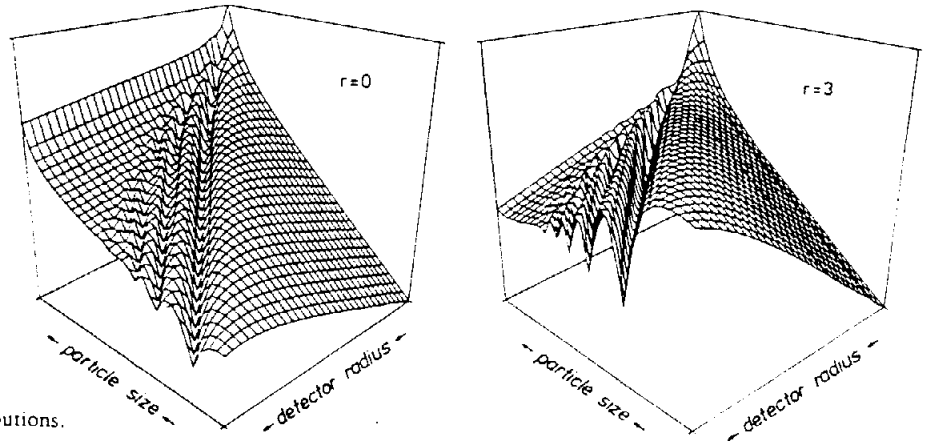

Fig. 7: Matrices for number and volume distributions.

of the diffraction picture outside the zero order. The smoothness on the edge of the matrix for large particles results from the fact that the particle size intervals of the integration continually become larger for a logarithmic subdivision of the axes.
The peaks and valleys project more for smaller integration intervals, that is the more equations and detector elements one uses. The values for large particles and small radii disappear from the presentation since the inner circular rings of the detector are proportionally too wide for manufacturing reasons.
One recognizes that the matrix obtained for a number distribution ($r = 0$) has its largest values on its outer edge for large particles. On the other hand, the matrix obtained for a volume distribution ($r = 3$) exhibits the desired form. The largest values lie near the main diagonal and are nearly of the same size.

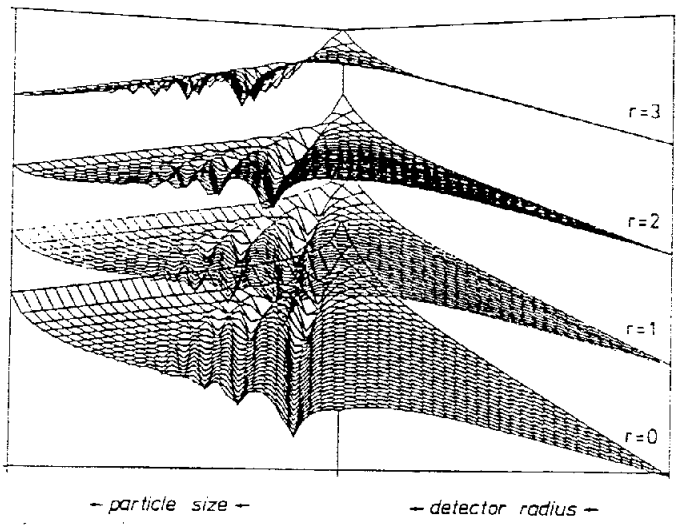

Fig. 8: Matrices for number and volume distributions.

In Figure 8 the matrices for the four quantity types $r = 0$ to $r = 3$ are presented in a somewhat different fashion. If one observes the form of the surfaces with increasing type of quantity, one recognizes the change from a lateral matrix emphasizing large particles at $r = 0$ to a matrix with $r = 3$ with values in the region of the main diagonals being approximately the same. The surface drops on both sides of the main diagonals.

5 Description of the Instrument

For the measurements described, a modular diffraction spectrometer HELOS * was built, which consists of the following major components:

1. The system for obtaining the test data: It is set up on an optical bench and includes all components for the production of the diffraction pattern, such as:
   - laser
   - expansion optics
   - mirror system
   - collection lens
   - multielement detector
   - suspension cell or the feeder-dispersion system RODOS * for dry powders.
2. The system for the processing of the test data: It consists of a Kontron microcomputer PSI 82 which contains all components necessary for the reception, corroboration, and processing of the data.
3. The delivery units, printer and plotter.

The test data are obtained from the computer by means of a "sample and hold" hook up, thus levelling the oscillations of the test signal caused by concentration- and laser power oscillations.

* Manufactured by: SYMPATEC GmbH, Asseweg 18, D-3346 Remlingen (Federal Republic of Germany).

6 Results obtained in the Experiment

6.1 Measurement of Latexes

In order to check the conformity of the analyzed distribution curves for spherical, absorbing particles, narrow sized latex suspensions covering a particle size range from 2 µm to 42 µm were analysed with the instrument. The latex suspensions used were obtained from the firm Coulter Electronics, Luton, England. After agitating the samples an appropriate amount of latexes were transferred to the suspension cell of the instrument and dispersed using ultrasonics for appr. 30 seconds. The distribution was then analysed running the instrument for 20 seconds. During this time the diffraction pattern was scanned 6666 times. In Figure 9 the average data given by Coulter Electronics, that is: $x_{50,V}$ the weight peak split (comparable with the most frequent value of $q_3(x)$) and $x_{50,0}$ the so called singlet number median diameter, are compared with the mode x_h and the median particle size $x_{50,3}$ of $q_3(x)$, obtained with the diffraction analyser.

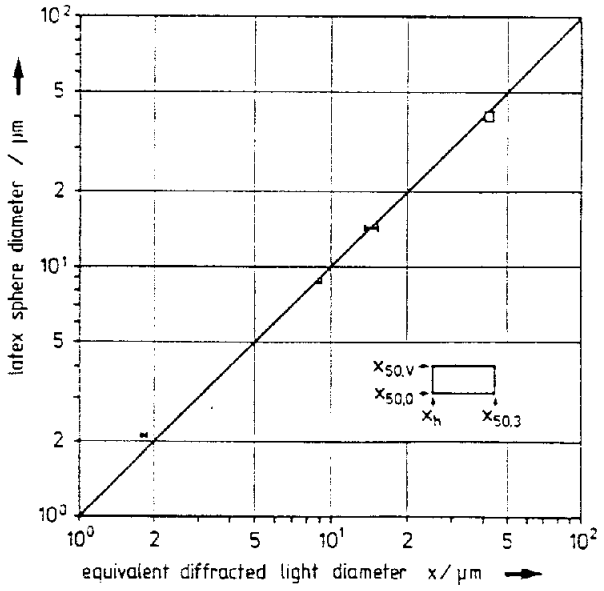

Fig. 9: Comparison of results obtained from diffraction pattern analyses with latex.

The mode x_h, the most frequent particle size obtained with diffraction pattern analysis, agrees within 1,5% with the $x_{50,V}$ values of the 8.7, 14.1 and 39.5 µm latexes. With the 2.11 µm latex sample the diffraction pattern results give smaller sizes, which was to be expected in the border region of Fraunhofer diffraction.

6.2 Investigation of the Reproducibility of the Results

In order to investigate the reproducibility of the results obtained with the instrument, measurements were performed with a lime-

stone distribution covering a size range between 2 and 40 µm. The results, from repeated measurements of one, and of several different samples are presented in Figure 10. The repeated measurements of one sample, shown on the left hand side of Figure 10, produced standard deviations of less than 0.36%. These deviations are given in Figure 10 for four points of the density distribution.

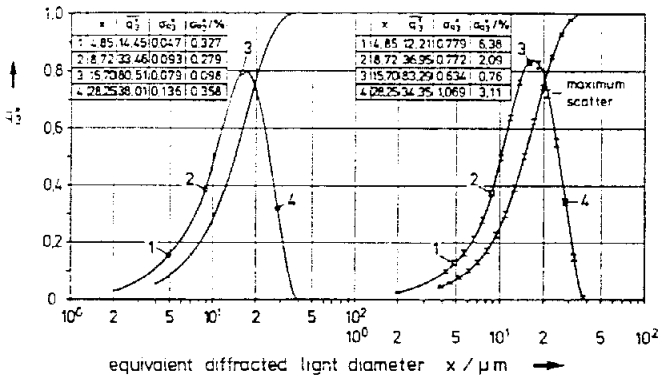

Fig. 10: Scatter of results obtained from repeated measurements of the same and of different limestone size distributions.

The standard deviation of measurements of different samples was approximately ten times larger. On the right hand side of Figure 10, the same particle size distribution is shown displaced two powers of ten from the distribution on the left. The vertical lines shown at different points give the maximum scatter band, caused by the error introduced when splitting the original sample.
In order to obtain an adequate, statistically reliable result, there must be a certain minimum number of particles in the laser beam when measuring the distribution. On the other hand, the solids concentration should not be too high in order to keep multiple scattering as small as possible.
Density and cumulative distribution curves for optical concentrations between 0.275 and 0.541 have been plotted on the left hand side of Figure 11. One discerns a small displacement to smaller particles, in the fine region, with increasing solids concentration. The overall deviation is very small and is presumably due to multiple scattering and diffraction.

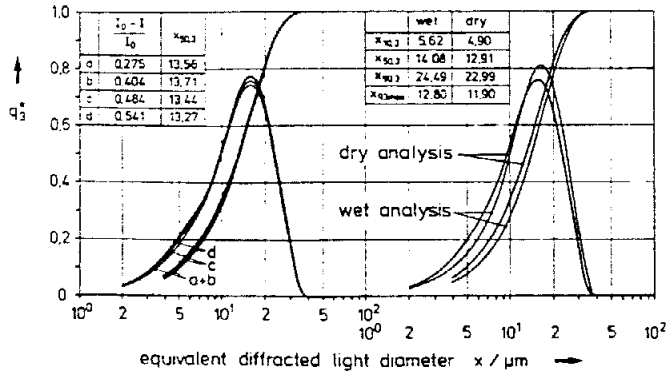

Fig. 11: Comparison of results obtained at optical concentrations between 0.275 and 0.541 and of wet and dry analyses.

The measurements so far presented were carried out with suspensions. In many cases, however, it is difficult, or nearly impossible, to find an appropriate liquid or a suitable dispersion medium for a certain solid. In other cases one is interested in the agglomerate size distribution in a dry condition. *Leschonski, Röthele* and *Menzel* [13] have, therefore, developed and tested a dry feeder-dispersion unit, which produces an aerosol as a free jet to be blown through the laser beam. A comparison of the density and cumulative distributions, as obtained by dry analysis, with the ones obtained with a suspension is represented on the right hand side of Figure 11. One sees a small displacement of the distribution curves of the dry samples towards finer sizes compared to the wet analysis.
The instrument can be operated with different focal lengths of 50 mm, 200 mm, and 1000 mm. Measurements in particle size ranges below 100 µm, 400 µm or 2000 µm can thus be carried out. Figure 12 shows the result as obtained with the same latex distribution using different focal lengths of 200 mm and 1000 mm. One sees a shift of the distribution towards finer sizes on the fine end of the distribution for the smaller focal length. In the upper region the density curves agree. This effect can be traced back to the small spread of the lobe and the collection of several secondary maxima of the intensity distributions of the particles at lower focal distances.

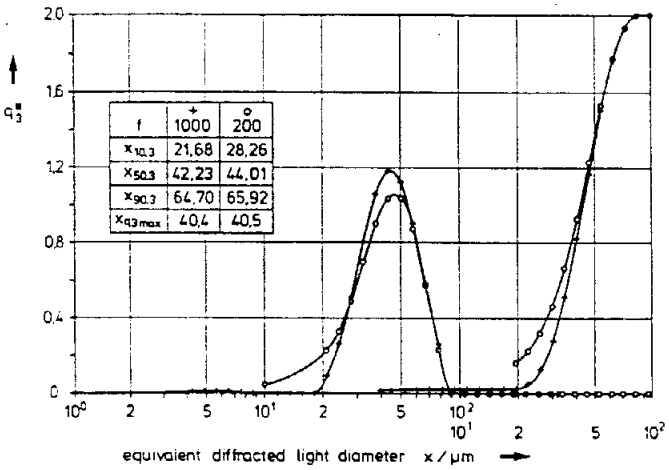

Fig. 12: Comparison of results obtained with focal distances of 1000 mm and 200 mm of the same latex suspension.

6.3 Results from Measurements of Mixtures

A particularly difficult test for instruments used for particle size analysis is the measurement of bimodal distributions. For this purpose, two primary limestone distributions in the particle size range from 2 µm to 10 µm and from 5 µm to 40 µm were first measured separately, and then with mixture ratios of 10:90, 30:70, 50:50, 70:30 and 90:10. The measured curves of the mixtures were then compared with the curves calculated from the primary distributions. The results are shown in Figure 13.
The measured distributions for the 10:90, 30:70, and 50:50 mixtures agree well with the curves calculated from the primary distributions within the thickness of the lines. This represents an absolute error of approximately 0.5%. The measured 70:30 distribution agrees in the upper and lower region and shows a slight deviation in the middle region (the maximum deviation amounts to 2.67% absolute from Q_3). The measured 90:10 distribution is shifted towards the finer sizes throughout the entire particle size range. The maximum absolute deviation amounts to 4%. The deviation observed is presumably caused by too small a number of coarse particles.
As a further example, the primary distributions of two quartz fractions and their 50:50 mixture are shown in Figure 14.

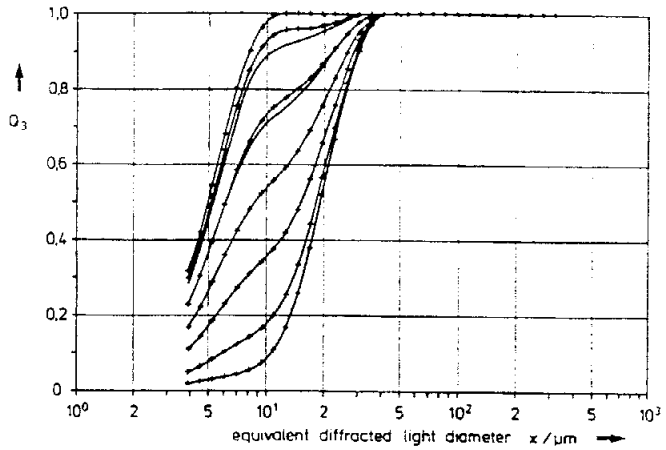

Fig. 13: Comparison of size distributions as obtained from limestone-mixtures.

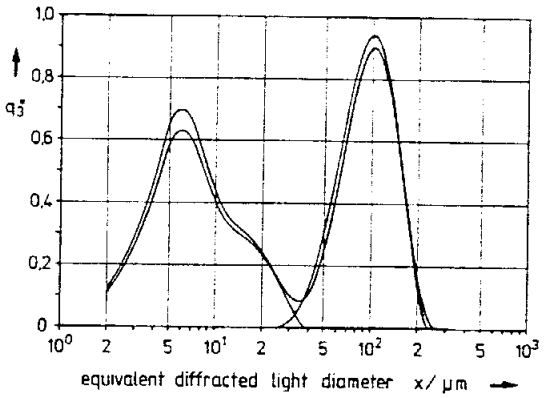

Fig. 14: Primary- and 50 : 50-mixture-distribution of quartz fractions.

7 Summary

If one uses a large number of support points when measuring a particle size distribution from a diffraction pattern, the use of a special mathematical method is unavoidable for the evaluation of the particle size distribution. The solution method, initially proposed by *Phillips* [9] and *Twomey* [10], contains no restrictions to the number of possible solutions. The process described is suitable for on-line measurements.

8 Symbols and Abbreviations

a	vector of the deviations
a_i	deviation
A	coefficient matrix
e	error vector
f	focal length
f_g	area error of the density curve
H	smoothness matrix
I	intensity of light
I_0	initial intensity of light
J_0	Bessel function of zero order
J_1	Bessel function of first order
$k = (\pi/\lambda f)$	abbreviation
K	deviation matrix
L	power of the light
M	number of particle size intervals
N_{tot}	total number of the particles
q	density distribution
Q	cumulative distribution
r	radius
s	standard deviation
x	particle diameter
x_{50}	median of cumulative distribution
x_h	mode of the $q_3(x)$ distribution
γ	Langrange multiplier
Δr	ring width
λ	wavelength
θ	diffraction angle

Indices

e	exact
f	error afflicted
g	smoothed
tot	entire
i	running variable for particle sizes
j	running variable for detector radii
max	maximum
min	minimum
r	type of quantity
T	transposed

9 References

[1] *J. Fraunhofer:* Bestimmung des Brechungs- und Farbzerstreuungsvermögens verschiedener Glasarten. Gilberts Annalen der Physik *56* (1817) 193 – 226.

[2] *G. B. Airy:* On the diffraction of an object glass with circular aperture. Trans. Camb. Phil. Soc. *5* (1835) 283 – 290.

[3] *J. H. Chin, C. M. Sliepcevich, M. Tribus:* Particle size distributions from angular variation of intensity of forward scattered light at very small angles. J. Phys. Chem. *59* (1955) 841 – 844.

[4] *J. H. Chin, C. M. Sliepcevich, M. Tribus:* Determination of particle size distributions in polydispersed systems. J. Phys. Chem. *59* (1955) 845 – 848.

[5] *K. S. Shifrin:* Trudy VZLTI (Leningrad) *2* (1956) 153 – 162.

[6] *E. C. Titchmarsh:* Introduction to the theory of fourier integrals, Claredon Press, Oxford 1924.

[7] *K. S. Shifrin, I. B. Kolmakov:* Izv, Acad. Sci, USSR, Atmos. Oceanic Phys. *2* (1966) 851 – 857.

[8] *S. Twomey:* On the numerical solution of fredholm integral equations. J. Assoc. Comput. Mach. *10* (1963) 97 – 101.

[9] *B. L. Phillips:* A technique for the numerical solution of certain integral equations of the first kind. J. Assoc. Comput. Mach. *9* (1962) 84 – 87.

[10] *S. Twomey:* Introduction to the mathematics of inversion in remote sensing and indirect measurements. Elsevier, Amsterdam 1977.

[11] *M. Heuer:* Verfahren zur Berechnung von Partikelgrößenverteilungen aus Beugungsspektren. 3. Fachtagung "Granulometrie 1983" Dresden.

[12] *K. Leschonski, W. Alex, B. Koglin:* Darstellung und Auswertung von Teilchengrößenverteilungen. Chem. Ing. Tech. *46* (1974) 23 – 26.

[13] *K. Leschonski, S. Röthele, U. Menzel:* Entwicklung und Einsatz einer trockenen Dosier-Dispergiereinheit zur Messung von Partikelgrößenverteilungen in Gas-Feststofffreistrahlen aus Beugungsspektren. 3. Fachtagung "Granulometrie 1983" Dresden. Part. Charact. *1* (1984) 161 – 166.